NASA Technical Memorandum 88975

Experimental and Analytical Evaluation of Dynamic Load and Vibration of a 2240-kW (3000-hp) Rotorcraft Transmission

Fred K. Choy, Dennis P. Townsend,
and Fred B. Oswald
Lewis Research Center
Cleveland, Ohio

Prepared for the
Design Engineering Conference and Show
sponsored by the American Society of Mechanical Engineers
Chicago, Illinois, March 2–5, 1987

NASA

EXPERIMENTAL AND ANALYTICAL EVALUATION OF DYNAMIC LOAD AND VIBRATION OF A 2240-kW (3000-hp) ROTORCRAFT TRANSMISSION

Fred K. Choy,* Dennis P. Townsend, and Fred B. Oswald
National Aeronautics and Space Administration
Lewis Research Center
Cleveland, Ohio 44135

SUMMARY

A dynamic analysis of a 2240-kW (3000-hp) helicopter planetary system is presented. Results from both analytical and experimental studies show good correlation in gear-tooth loads. A parametric study indicates that the mesh damping ratio has a significant effect on maximum gear-tooth load, stress, and vibration. Correlation with experimental results indicates that the sun-planet mesh damping ratio can significantly differ from the planet-ring mesh damping ratio. A numerical fast Fourier transform (FFT) procedure was applied to examine the mesh load components in the frequency domain and the magnitudes of multiple tooth-pass frequencies excited by nonsynchronous meshing of the planets. Effects of tooth-spacing errors and tooth-profile modifications with tip relief are examined. A general discussion of results and a correlation with the experimental study are also presented.

INTRODUCTION

In helicopter (and other) gear transmissions there is a considerable amount of noise generated by the gear teeth as they transmit the load at the operating speed. This noise is the result of dynamic tooth loads that transmit vibration to shafting and structural elements of the transmission. Several methods have been tried in an attempt to reduce or eliminate the dynamic load and gear noise. Terauchi et al. (1982) showed that the noise level of a gear mesh could be reduced about 5 dB by using profile modification (tip relief). Changing the contact ratio from less than 2 to between 2 and 3 should reduce the dynamic tooth loads by keeping the gear-tooth spring rate more uniform (Welbourn, 1977), thereby causing a more uniform load transmission between gear teeth.

Several years ago it was decided to investigate the effects of high-contact-ratio gears and gear-tooth-profile modifications on the dynamic tooth loads. The investigation included both an experimental and an analytical evaluation of dynamic gear loads for standard and high-contact-ratio gears (i.e., ratios greater than 2) (Cornell and Westervelt, 1978; Cornell, 1981). The initial analytical results were used to design test gears for an experimental testing program. Gear models with constant tooth-mesh stiffness did not give the best design: gear-tooth bending failures were experienced during the testing program. Consequently, the analytical program was modified to

---

*Summer Faculty Fellow; presently at The University of Akron, Akron, Ohio.

include variable tooth stiffness and various methods of tooth-profile modification. This improved analysis gives much better correlation with experimental results.

The initial analytical program was a single mesh spur-gear dynamic analysis. Since most helicopter transmissions utilize a planetary gear system, the program was expanded into a multiple mesh gear dynamic analysis that would determine the dynamic loads in the sun-planet and ring-planet meshes of a planetary gear system with several planets.

The program was developed for a planetary system with either standard or high-contact-ratio gears and with either spur or helical gears. The objective of the work reported herein was to use the planetary gear dynamic analysis program to evaluate a 2240-kW (3000-hp) planetary transmission and to compare the results of the program with experimental test data.

EXPERIMENTAL APPARATUS AND PROCEDURE

Test Transmission

The UH-60A helicopter transmission has a twin (T700) engine power rating of 2100 kW (2828 hp). It provides 81.042:1 total speed reduction in three stages from the engine inputs (20 900 rpm) to the rotor output (258 rpm). There is also a tail shaft output (4117 rpm).

The transmission (figs. 1 and 2) consists of two input modules and one main module. The input modules contain the first reduction stage - a 22-tooth spiral-bevel input pinion driving an 80-tooth gear. The gear rotates with an internal overrunning ramp roller clutch which drives a shaft leading to the main module of the transmission. The second reduction stage of the transmission consists of two 17-tooth combining spiral-bevel pinions which drive a single 81-tooth combining gear. This gear is splined to a 62-tooth sun gear from the planetary stage (third reduction). The sun gear drives five 83-tooth planetary gears which revolve with their carrier within the stationary 228-tooth ring gear. The helicopter main rotor is driven directly from the planetary carrier. Tail rotor power is taken from a 116-tooth spiral-bevel gear (on the back side of the combining gear) which drives a 34-tooth pinion. The total main-rotor speed reduction is

$$\frac{80}{22} \times \frac{81}{17}\left(1 + \frac{228}{62}\right) = 81.042$$

Instrumentation

The NASA Lewis Research Center 2200-kW (3000-hp) helicopter transmission test facility (fig. 3) is a recirculating (four square) facility. Power to the test transmission flows through two inputs (simulating two engines) and two outputs (main rotor and tail drive). Power is provided by a constant-speed 600-kW induction motor. Since power flow is recirculating, only frictional losses need be replenished by the motor. Speed control is provided by an eddy-current clutch. Torque (and hence circulating power) is induced independently in each loop by two-stage planetary torque units. The test facility is more fully described by Mitchell et al. (1986).

The strain gauges are general-purpose electrical-resistance constantan foil gauges. Gear-tooth gauges have a gauge length of 0.38 mm (0.015 in.). Strain-gauge signals from the rotating sun gear are fed out through an internal slipring.

PROCEDURE

Twenty strain gauges were installed on the teeth of the sun and ring gears. To measure maximum tooth bending stresses, fillet gauges were placed at the 30° tangency location (fig. 4) on the loaded side of the tooth fillet. To measure rim bending stresses, root gauges were placed in the center of the tooth root. Each instrumented tooth had five gauges spaced evenly across the face width. On the sun gear, one tooth was instrumented with root gauges. On the ring gear, two consecutive teeth were instrumented with fillet gauges and one tooth was instrumented with root-gauges. All gauges were mounted along the plane normal to the tooth surface (the plane of rotation) in the assumed principal stress direction.

Strain-gauge readings were measured with constant-current dynamic strain-gauge-amplifiers. The signal from the strain amplifiers was stored on 14-channel FM tape for later analysis using an analog to digital converter (ADC) and a microcomputer. A five-range T-bar switch was used to record 50 strain-gauge signals on a single 14-channel tape. Signals were low-pass filtered to reduce slipring noise.

Analytical Approach

The dynamic model for the multimesh planetary system, which was based on that developed by Richardson (1958) and Howland (1962), was recently expanded to cover larger contact ratios (Cornell and Westervelt, 1978; Cornell, 1981). In this analysis, the variation of tooth-pair compliance with position along the line of action is defined by a five-term power series:

$$\frac{\bar{C}}{\bar{C}_0} = 1 + A\frac{S}{S_0} + B\left(\frac{S}{S_0}\right)^2 + C\left(\frac{S}{S_0}\right)^3 + D\left(\frac{S}{S_0}\right)^4 \qquad (1)$$

where $\bar{C}_0$ is the compliance at the pitch radius; A, B, C, and D are the gear compliance coefficients; and S and S_0 are, respectively, the relative motion and the reference distance along the line of action. The gear load can be calculated by solving the equations of relative motion between two gears (Cornell and Westervelt, 1978; Cornell, 1981) and by assuming a rigid ring and planet carrier. For a multimesh planetary system, initial boundary displacements and velocities are approximated to solve the equations of motion (Pike, 1981; Boyd and Pike, 1985). An iterative scheme is set up to calculate the final gear load and boundary conditions.

RESULTS AND DISCUSSIONS

A parametric study of the effects of damping ratios on the UH-60A Blackhawk 2240-kW (3000-hp) transmission was performed to provide a more consistent correlation of the analytical simulations to the experimental

results and to achieve a better understanding of the dynamic behavior of the system. Figures 5 and 6 present the dynamic tooth load and maximum bending stress, respectively, of the first sun-planet mesh along the line of action for a range of mesh damping ratios C from 0.02 to 0.20. Note that the dynamic tooth load, hertz stress, and maximum bending stress all possess similar characteristics as the mesh damping ratio changes. In this particular case, four dominant peak components are observed at low damping ratio during one single tooth pass. With the increase in damping ratio, the peaks become less pronounced, and they are almost undetectable at higher damping.

The existence of the fourth-order single-tooth-pass frequency harmonic is due to the nonsynchronous meshing of the other planets. Table I shows the phasing constants for various planets. Note that with light damping the maximum loads for the sun-planet mesh occur close to the phasing constant values. As the damping increases, the locations of the maximum load and stress begin to shift. Since the loads and stresses shown in figures 5 and 6 are from the first mesh, it is logical to assume that more dominate effects would be obtained at the phasing locations of its neighboring planets: that is, the second and fifth mesh. A closer examination reveals that the total load is higher while individual load is lower because of multitooth participation in the mesh.

Figure 7 gives the dynamic loading on the ring-planet mesh while figure 8 gives the maximum ring-gear tooth bending stress during the tooth pass. Figures 7 and 8 also show harmonic frequency characteristics that are similar to the sun-gear stresses depicted in figures 5 and 6. A more pronounced phase delay can be observed from the ring-planet mesh load for large damping. This is because the sun gear is the driver and more direct action is imposed. Further confirmation of the fourth-order single-tooth-pass frequency can be achieved by using fast Fourier transform (FFT) techniques to examine the frequency components. Figure 9 depicts the mesh load for various damping ratios for 10 consecutive single tooth passes. The overlapping of the curves show the load participation of each tooth in the mesh. The frequency domain results are presented in figure 10. Note that in figure 9 the peak loads are much higher at smaller damping, as expected by any mechanical system. The average load shown in figure 10 is slightly lower at smaller damping ratios because there is a much larger load variation in a lightly damped system. As a result, the other meshes have to share a higher average load to compensate for the loss. In extreme cases light damping may even result in several cycles of complete disengagement-engagement of the gear tooth during one single tooth pass. It can also be seen that the fourth-order tooth-pass component (3900 Hz) is more pronounced with a decrease in damping, as predicted by the tooth load and stress analysis in figures 5 and 6.

Figure 11 shows the dynamic tooth load for the other four meshes with the tooth-spacing error at a low damping ratio (C = 0.02). A considerable variation can be observed in the dynamic tooth load at different meshes because of phasing. Note that the load vanishes several times in one single tooth pass for the second mesh, which indicates several engagement-disengagements occurred during a single tooth pass. During such a disengagement-engagement process, the maximum dynamic tooth load is greatly increased. As a result, system vibration and noise increase significantly.

Figure 12 depicts the frequency components of each mesh load. Note that the second mesh, which consists of several total disengagements during one single tooth pass, has the highest fourth-order tooth-pass frequency component. This indicates that a more dominating fourth harmonic of the tooth frequency can be expected. The average mesh loads remain moderately constant except for the fifth mesh, which is not heavily loaded because of phasing and tooth-spacing error.

The previous analytical simulations are compared to experimental data obtained from the test stand to verify the results. Figure 13 shows both the fillet and root stresses measured in the ring gear during tooth-pass interactions. Note that in figure 13(b) and (c) both maximum fillet and root stresses are of the same order of magnitude as demonstrated by Drago (1982) for gear systems under large loading. Because of the limitations constrained in the experimental results (only root stresses have been monitored for the sun gear), the root stresses will be used for the comparison with analytical results. Figure 13(d) presents a comparison of the analytical calculated maximum bending stress to the experimental root stress reading in the ring gear. Note that there are good correlations between the results with a mesh damping ratio of 0.02.

Figure 14 shows the average sun- and ring-gear root stress averaged over ten tooth-pass interactions with a filter cutoff frequency of 1800 Hz. The maximum compressive root stress for the sun gear is 516 MPa (74 ksi) and maximum tensile root stress for the ring gear is 409 MPa (72 ksi). The analytical simulations predict a maximum sun fillet stress of 495 Mpa (72 ksi) at $C = 0.02$ and 295 MPa (43 ksi) at $C = 0.2$, as shown in figure 6. It is expected that, under large bending stress at the gear tooth, the maximum root compressive stresses and the fillet tensile stresses should have similar orders of magnitude (Drago, 1982). The sun root stresses were measured at the center of the root. Figure 7 shows that the ring fillet tensile stress can vary from 450 MPa (65 ksi) at $C = 0.02$ to 310 MPa (45 ksi) at $C = 0.2$. The experimental data and the analytical results indicate that a sun-planet mesh damping ratio of $C = 0.02$ and a ring-planet damping ratio of $C = 0.1$ provide the best correlation. It is logical to assume the sun-planet mesh provides less damping because of the floating sun arrangement, which is agreeable from the previous results. A closer examination of the experimental data further confirms this assumption.

Figure 15 shows the unfiltered (filter set at 20 kHz) and unaveraged strain-gauge data of the ring root stress during a tooth-pass interaction. The zoom-in data in figure 15(b) reveal that oscillations of the maximum bending stress will occur as predicted by the analytical model in figure 7. The fewer number of peaks and the less pronounced maximum peaks are probably due to material damping which is not modeled in the analytical simulation.

Figure 16 presents a waterfall diagram of the gear-box accelerometer vibration data at various speeds. The speed indicated is the carrier speed. At full speed, the first to the fourth harmonics of the tooth-mesh frequency can be detected distinctly. Similar trends of the frequency components can be recognized in figure 12. The difference in the average acceleration g-level (load) data of figures 16 and 12 may be due to the damping of the bearing supports and to the gear-box structure. Natural frequencies are detected at carrier speeds of 100, 190, and 220 rpm (pinion speeds of 450, 880, and 990 rpm). Natural frequencies are predicted through maximum planet load by the analytical

model at 420, 700, and 900 rpm. The other frequencies appearing in the accelerometer data, which are not predicted by the analytical simulation, are due to the effects of other gear inputs that are not in the numerical model. Overall, the major dynamic behavior has been predicted closely by the computer simulation.

CONCLUSIONS

1. Results from both analytical and experimental dynamic studies of a 2240-kW (3000-hp) rotorcraft transmission are presented. Good mesh load correlations are obtained from the analytical approach with experimental data.

2. The value of the mesh damping ratio can greatly affect the maximum tooth load and stress during a single tooth pass. While light damping can increase the maximum tooth load significantly, the average load in the single tooth pass will remain constant or decrease slightly with a decrease in damping.

3. For a nonsynchronous meshing planetary system, the load-stress cycle on a tooth is excited by integer multiple harmonics of the tooth-pass frequency up to the number of planets minus one. The excitations at these multiple harmonic frequencies can be effectively examined in the frequency domain using a numerical fast Fourier transform (FFT) procedure.

4. Mesh damping ratios can be estimated better by correlating them with experimental data. Experimental testing of a 2240-kW transmission reveals that the sun-planet damping ratio is much smaller than the ring-planet damping ratio, hence sun-planet loads and stresses tend to be greater.

5. The present rigid sun assembly model without rim flexibility and material damping tends to predict higher maximum tooth load and stress.

REFERENCES

Boyd, L.S., and Pike, J., 1985, "Multimesh Gear Dynamics Program Evaluation and Enhancements," NASA CR-174747.

Cornell, R.W., and Westervelt, W.W., Jan. 1978, "Dynamic Tooth Loads and Stress for High Contact Ratio Spur Gears," Journal of Mechanical Design, Vol. 100, No. 1., pp. 69-76.

Cornell, R.W., Apr. 1981, "Compliance and Stress Sensitivity of Spur Gear Teeth," Journal of Mechanical Design, Vol. 103, No. 2, pp. 447-459.

Drago, R.J., 1982, "An Improvement in the Conventional Analysis of Gear Tooth Bending Fatigue Strength," AGMA P229.24.

Howland, J.S, 1962, "An Investigation of Dynamic Loads in Spur Gear Teeth," Master's Thesis, MIT.

Mitchell, A.M., Oswald, F.B., and Coe, H.H, 1986, "Testing of UH-60A Helicopter Transmission in NASA Lewis 2240-kW (3000-hp) Facility," NASA TP-2626.

Pike, J.A., 1981, "Interactive Multiple Spur Gear Mesh Dynamic Load Program," NASA CR-165514.

Richardson, H.H., 1958, "Static and Dynamic Load, Stress, and Deflection Cycles in Spur Gear Systems," Sc. D. Thesis, MIT.

Terauchi, Y., Nadano, H., and Nohara, M., Sept. 1982, "On the Effects of Tooth Profile Modifications on Dynamic Load and Sound Level of Spur Gears," Bulletin JSME, Vol. 25, No. 207, pp. 1474-1481.

Welbourn, D.B., 1977, "Gear Noise Spectra - A Rational Explanation," ASME Paper 77-DET-38.

TABLE I. - PLANET MESH PHASING CONSTANTS

Mesh	Sun-planet mesh, tooth pass ratio	Ring-planet mesh, tooth pass ratio
First	0	0
Second	.4	.6
Third	.8	.2
Fourth	.2	.8
Fifth	.6	.4

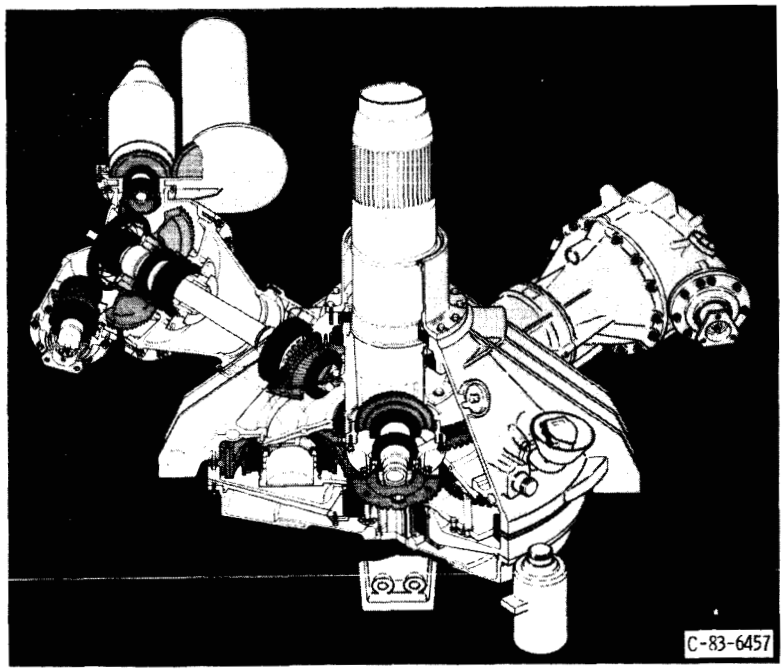

FIGURE 1. - ISOMETRIC VIEW OF UH-60A HELICOPTER TRANSMISSION.

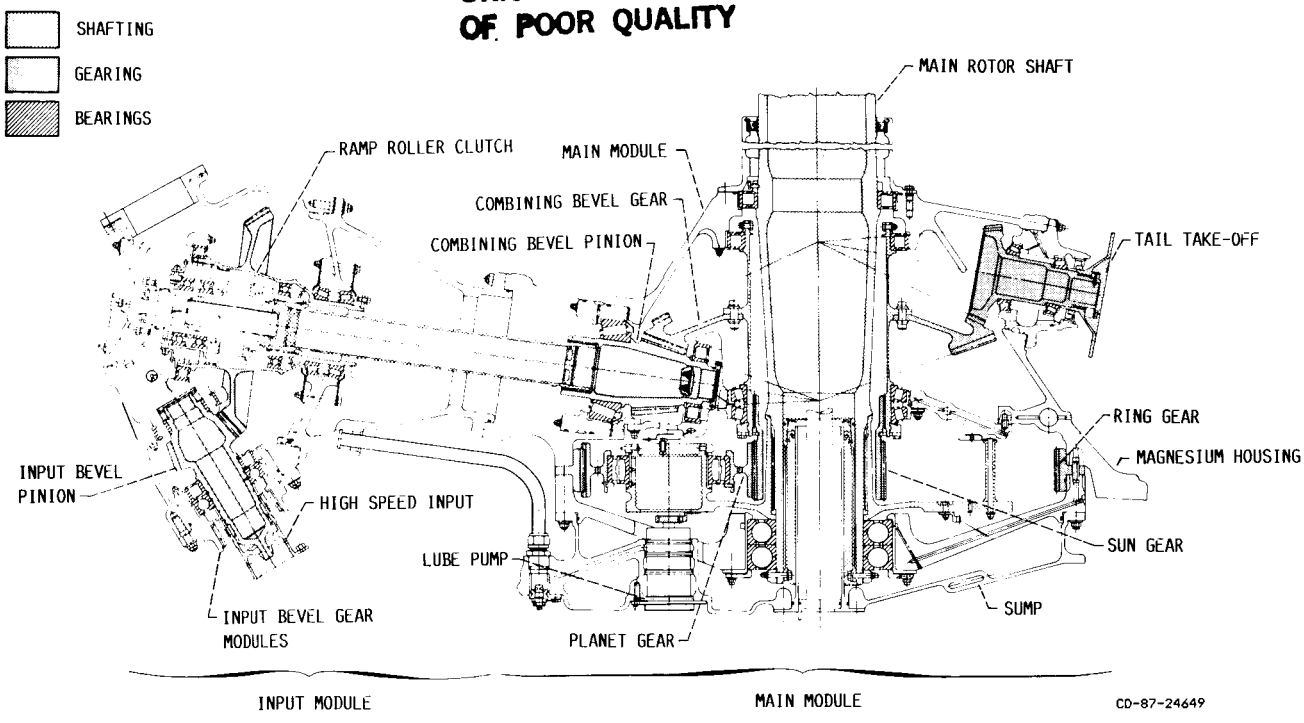

FIGURE 2. - CROSS SECTION OF INPUT MODULE AND TAIL OF UH-60A HELICOPTER TRANSMISSION.

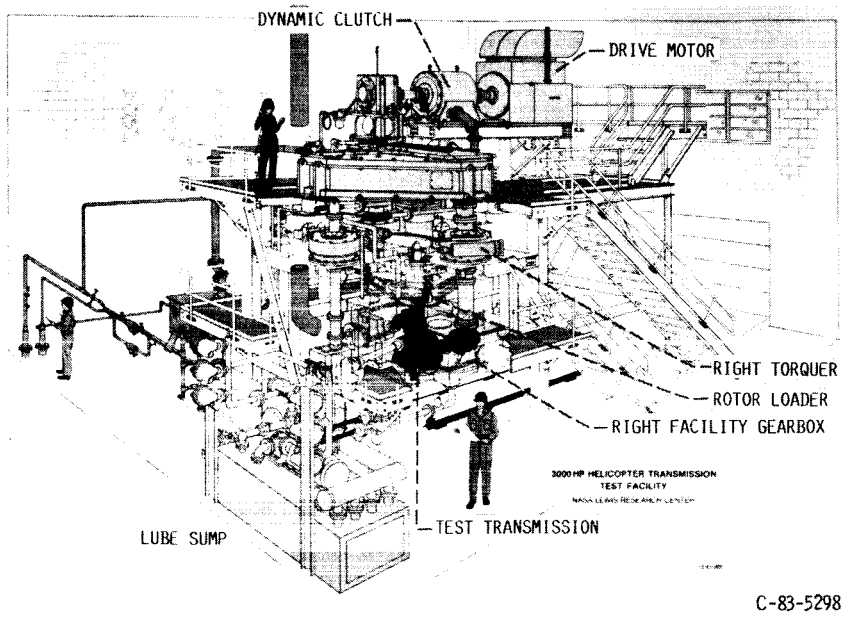

FIGURE 3. - NASA LEWIS RESEARCH CENTER 2240-kW (3000-HP) HELICOPTER TRANSMISSION TEST FACILITY.

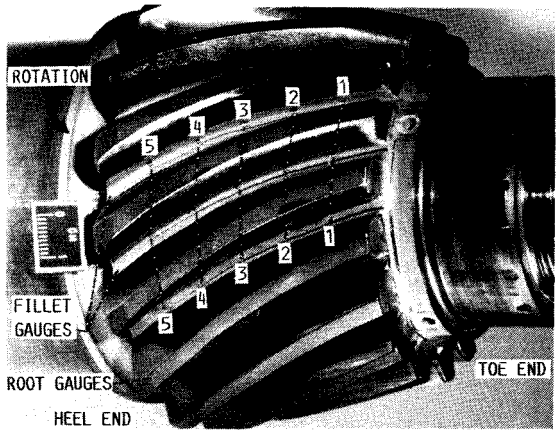

(A) PINION SHOWING GAUGE LOCATIONS.

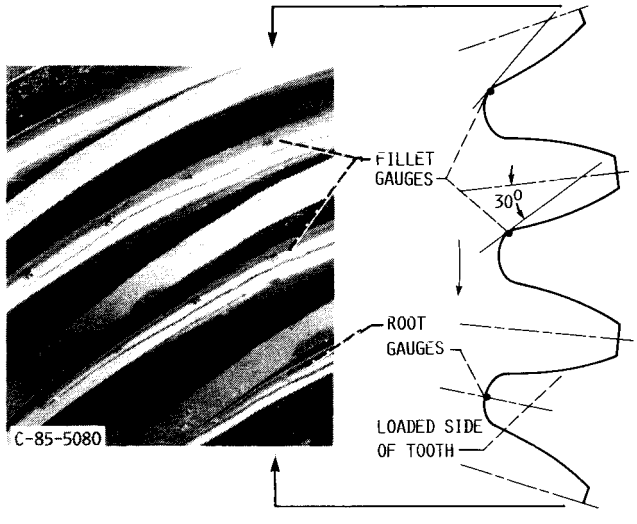

(B) PINION DETAIL.

FIGURE 4. - STRAIN-GAUGE INSTALLATION ON SPIRAL-BEVEL COMBINING PINIONS.

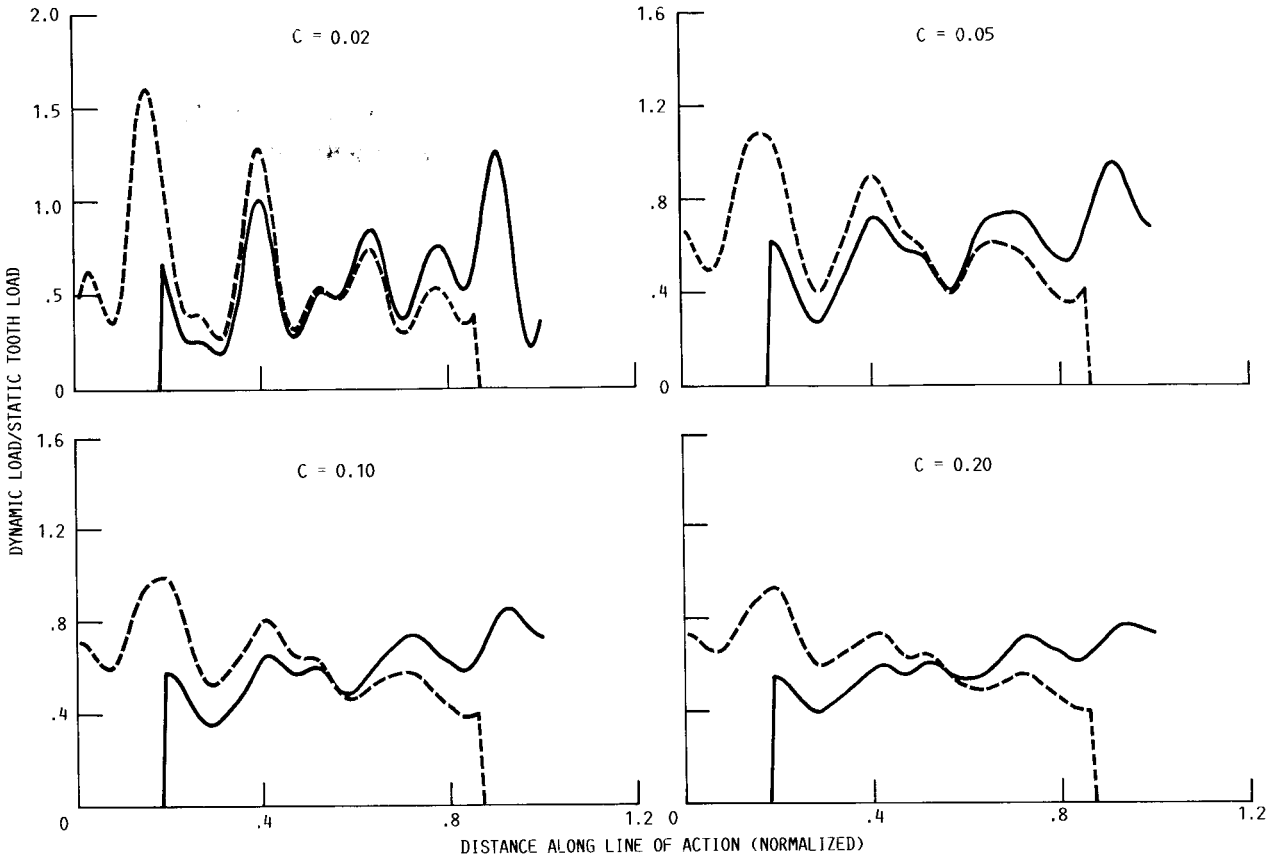

FIGURE 5. - EFFECTS OF MESH DAMPING RATIO C ON SUN-PLANET LOAD. SUN GEAR SPEED, 1206 RPM; INPUT TORQUE ON SUN GEAR, 15 000 N-M (11 000 LB-FT).

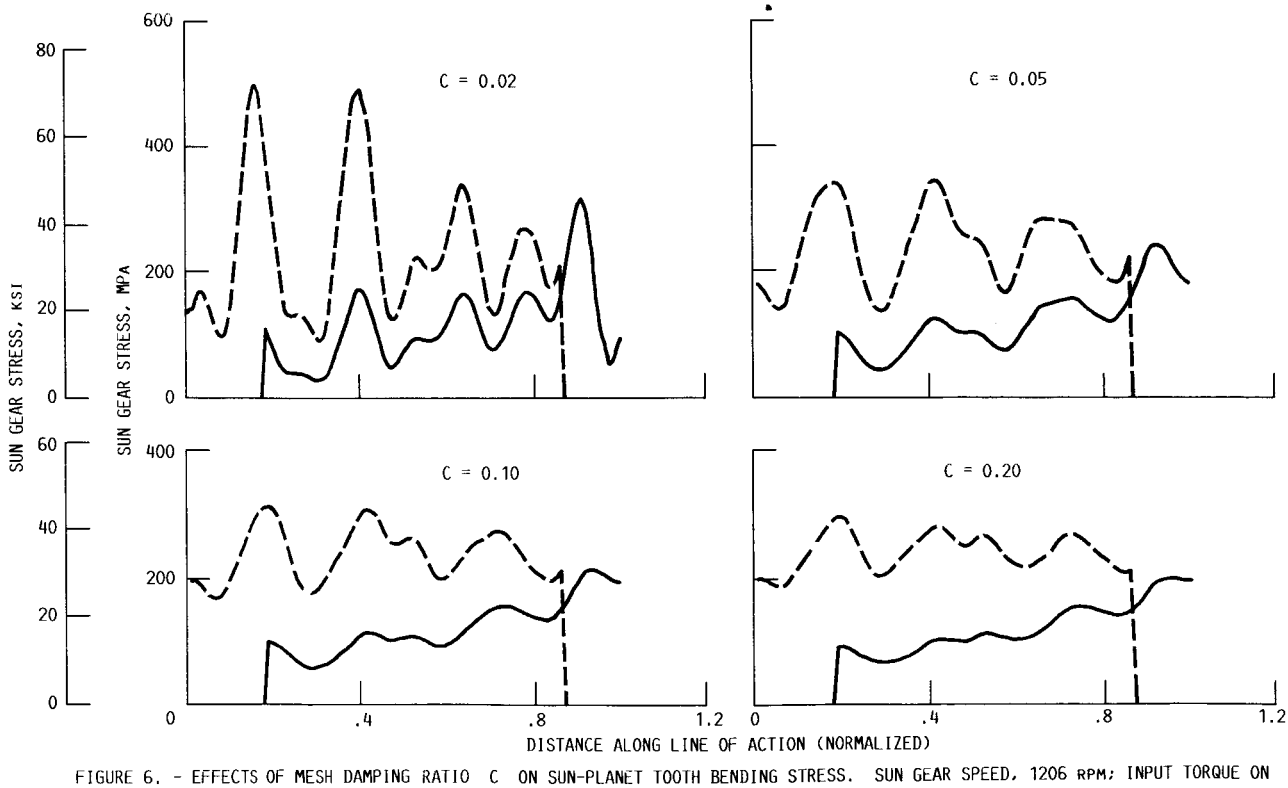

FIGURE 6. - EFFECTS OF MESH DAMPING RATIO C ON SUN-PLANET TOOTH BENDING STRESS. SUN GEAR SPEED, 1206 RPM; INPUT TORQUE ON SUN GEAR, 15 000 N-M (11 000 LB-FT).

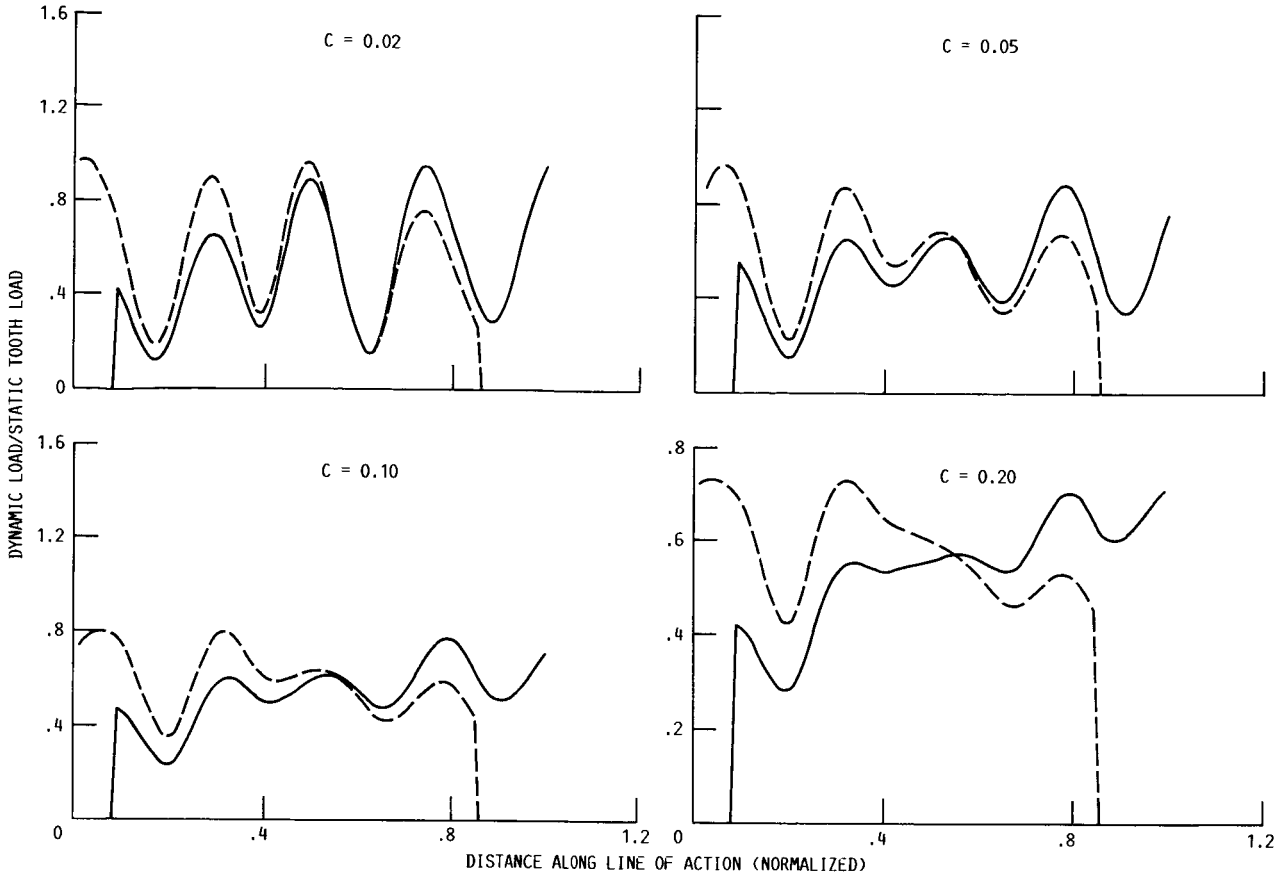

FIGURE 7. - EFFECTS OF MESH DAMPING RATIO C ON RING-PLANET LOAD. SUN GEAR SPEED, 1206 RPM; INPUT TORQUE ON SUN GEAR, 15 000 N-M (11 000 LB-FT).

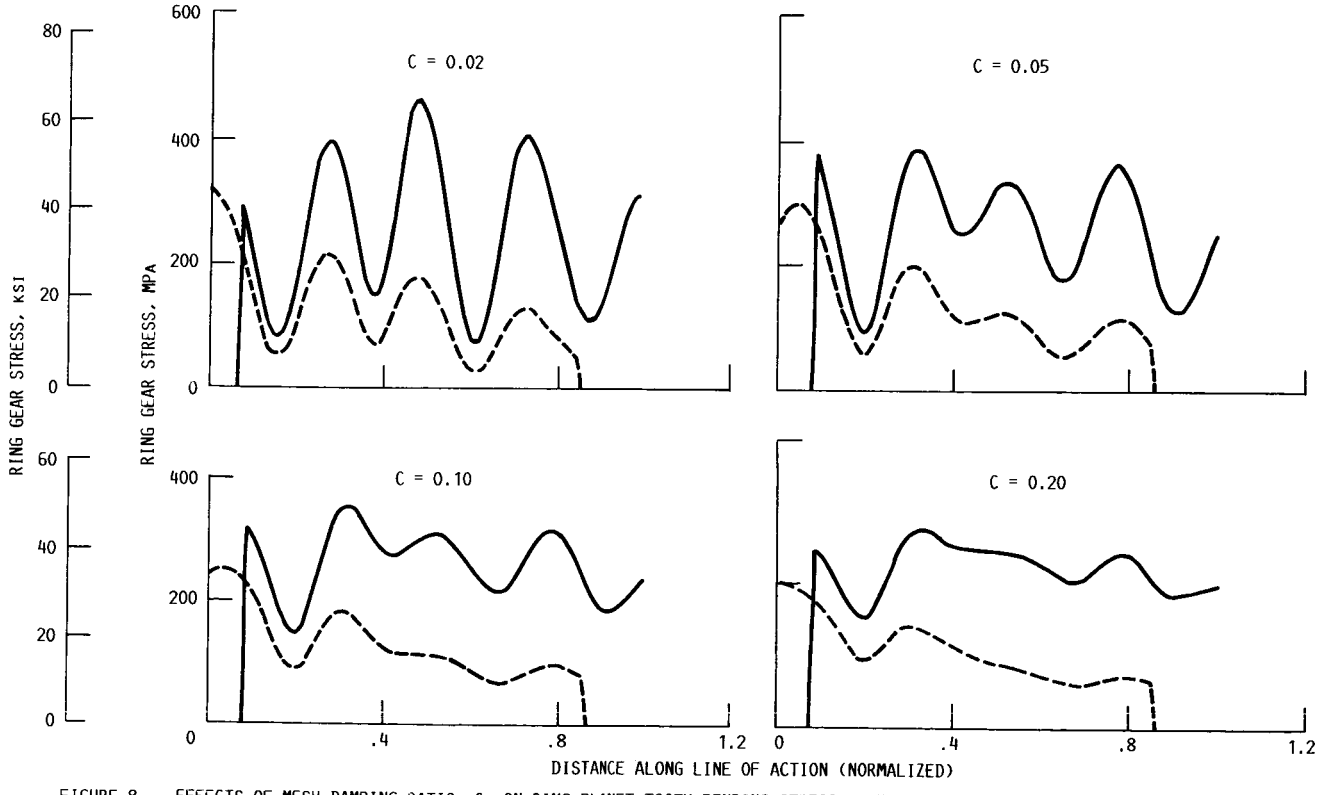

FIGURE 8. - EFFECTS OF MESH DAMPING RATIO C ON RING-PLANET TOOTH BENDING STRESS. SUN GEAR SPEED, 1206 RPM; INPUT TORQUE ON SUN GEAR, 15 000 N-M (11 100 LB-FT).

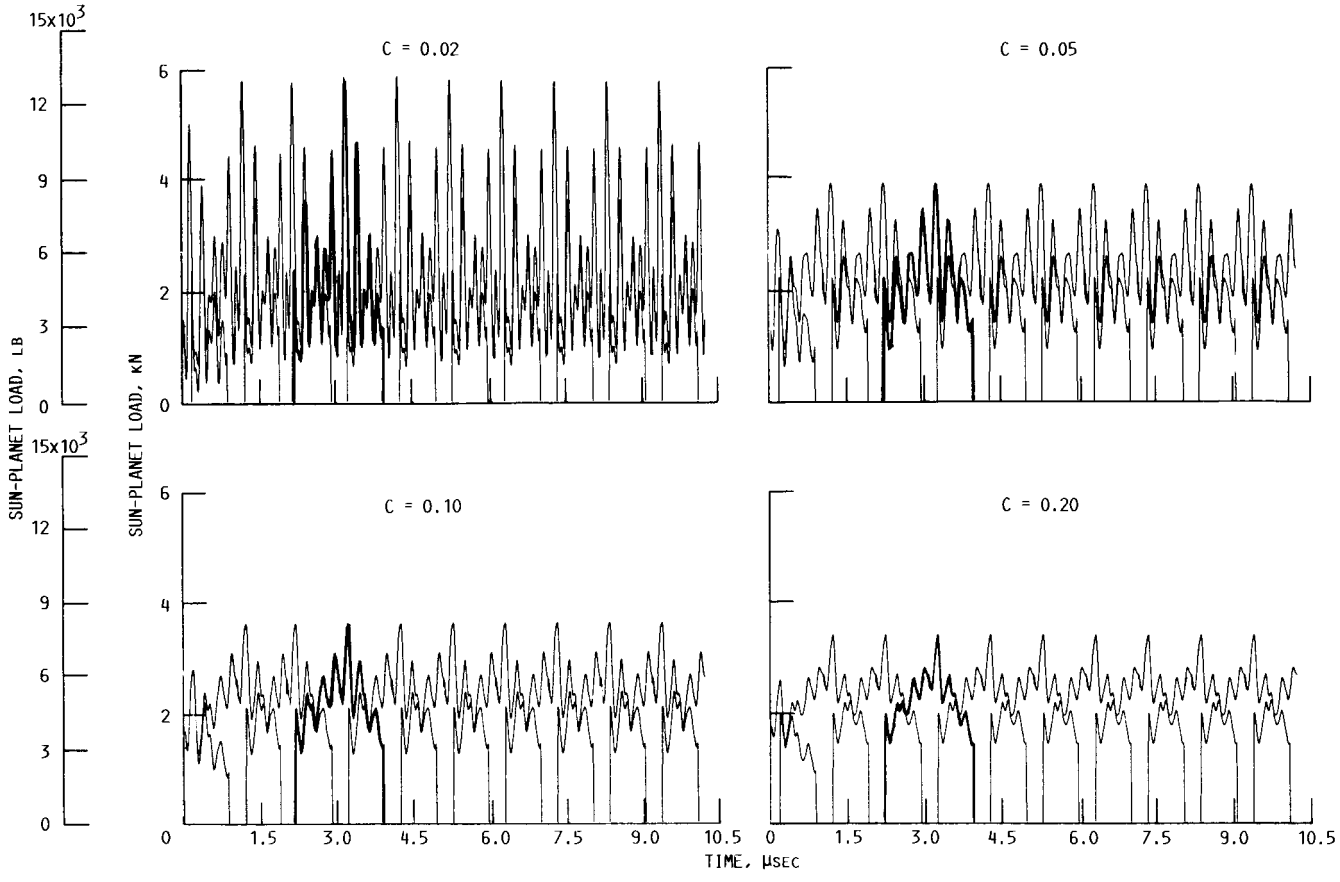

FIGURE 9. - EFFECTS OF MESH DAMPING RATIO C ON SUN-PLANET LOAD WITH TOOTH SPACING ERROR, SUN GEAR SPEED, 1206 RPM; INPUT TORQUE ON SUN GEAR, 15 000 N-M (11 100 LB-FT).

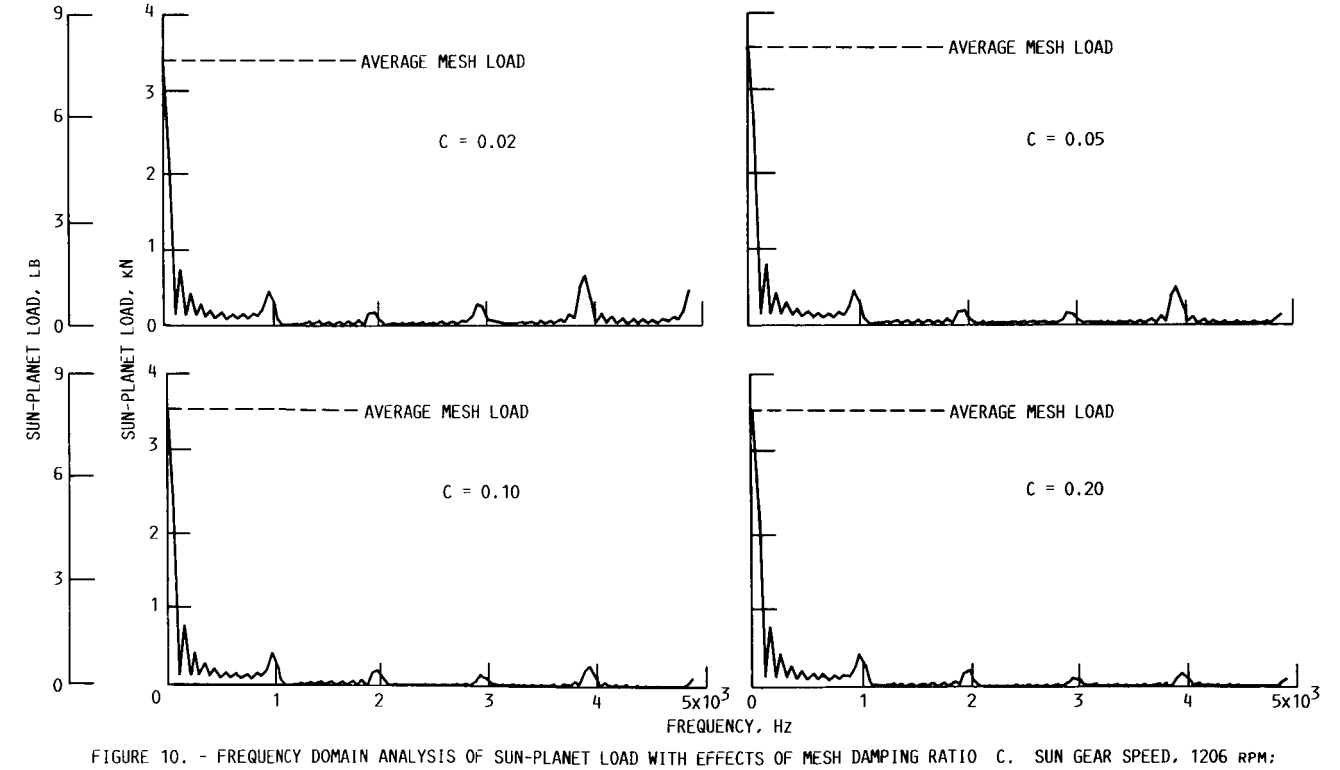

FIGURE 10. - FREQUENCY DOMAIN ANALYSIS OF SUN-PLANET LOAD WITH EFFECTS OF MESH DAMPING RATIO C. SUN GEAR SPEED, 1206 RPM; INPUT TORQUE ON SUN GEAR, 15 000 N-M (11 000 LB-FT).

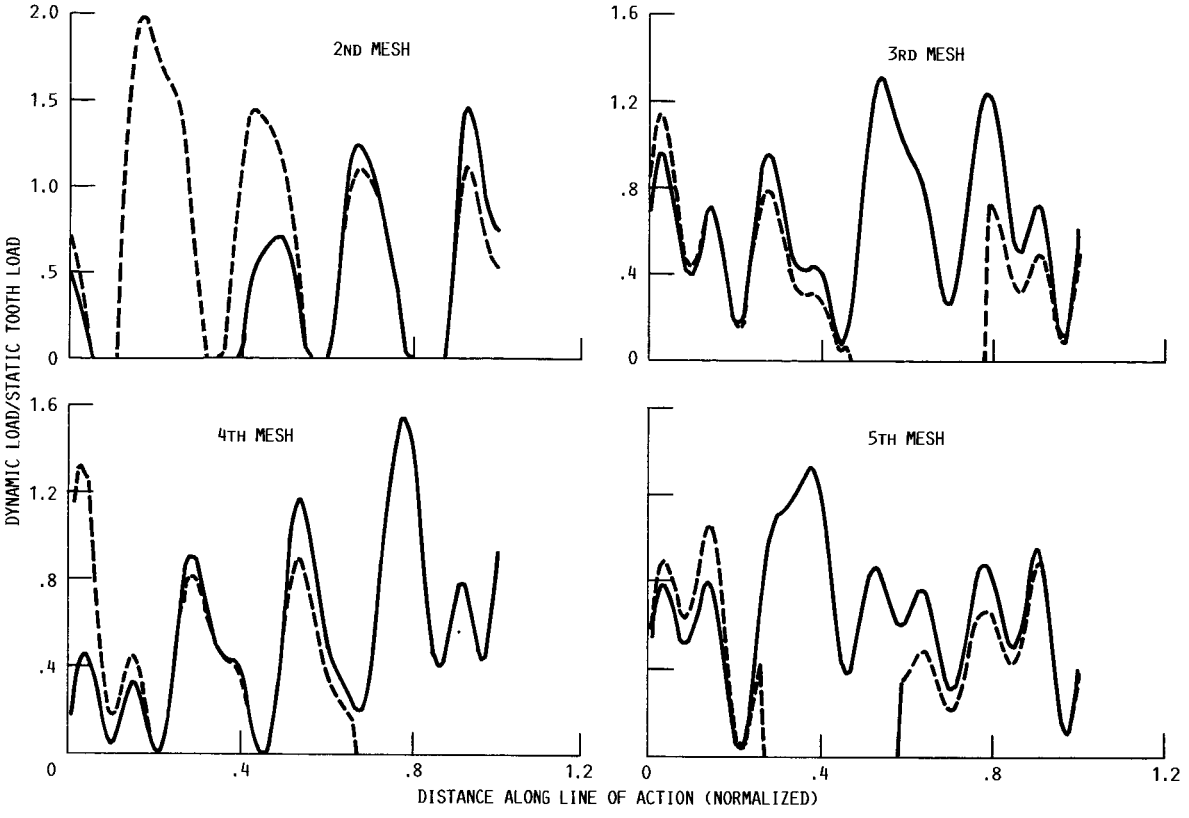

FIGURE 11. - SUN-PLANET LOAD WITH LIGHT DAMPING (C = 0.02) AT DIFFERENT PLANET LOCATIONS. SUN GEAR SPEED, 1206 RPM; INPUT TORQUE ON SUN GEAR, 15 000 N-M (11 000 LB-FT).

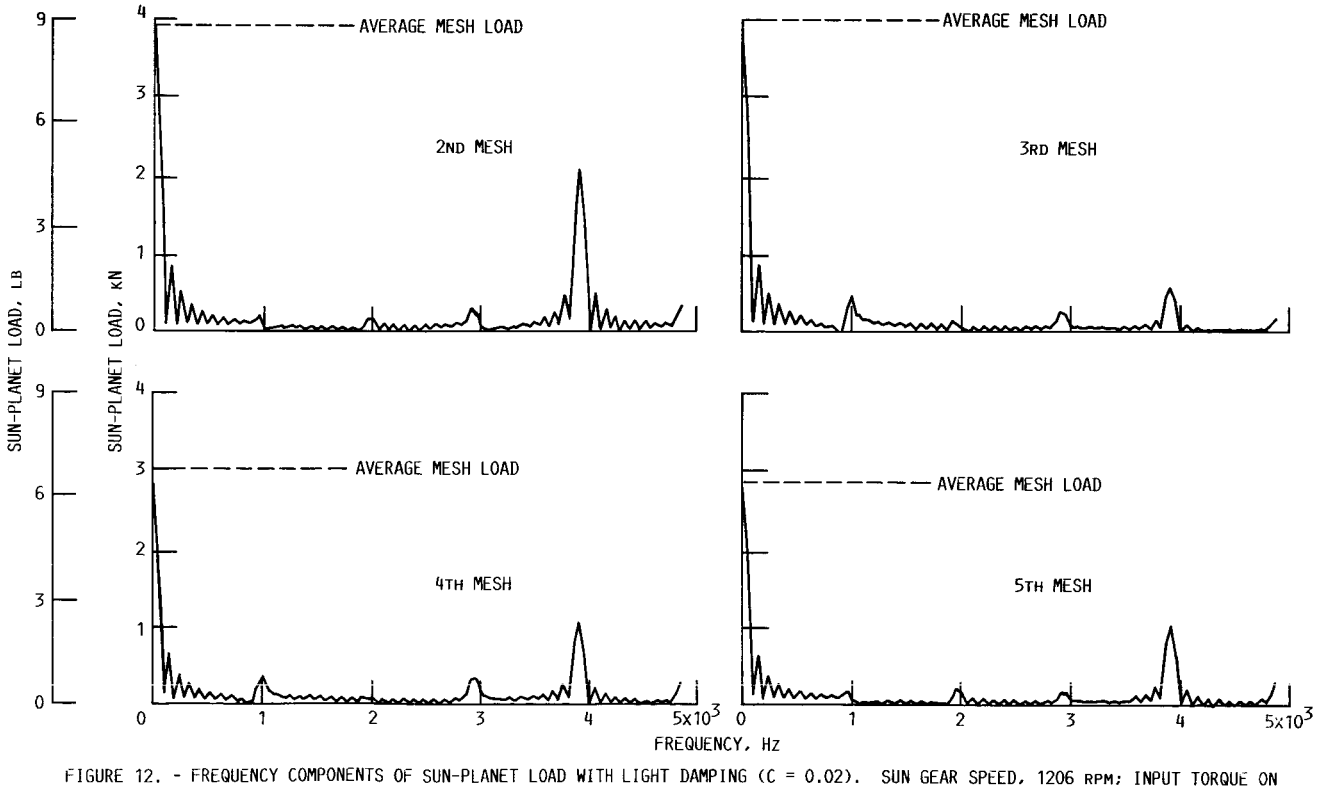

FIGURE 12. - FREQUENCY COMPONENTS OF SUN-PLANET LOAD WITH LIGHT DAMPING (C = 0.02). SUN GEAR SPEED, 1206 RPM; INPUT TORQUE ON SUN GEAR, 15 000 N-M (11 000 LB-FT).

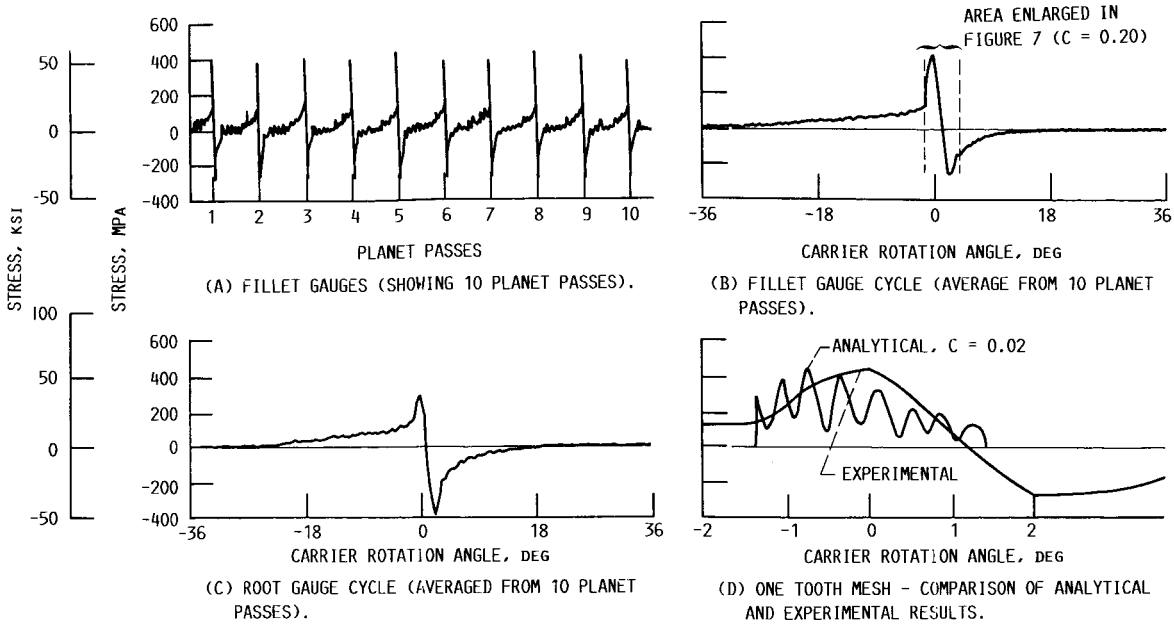

(A) FILLET GAUGES (SHOWING 10 PLANET PASSES).

(B) FILLET GAUGE CYCLE (AVERAGE FROM 10 PLANET PASSES).

(C) ROOT GAUGE CYCLE (AVERAGED FROM 10 PLANET PASSES).

(D) ONE TOOTH MESH - COMPARISON OF ANALYTICAL AND EXPERIMENTAL RESULTS.

FIGURE 13. - STRESS IN RING GEAR.

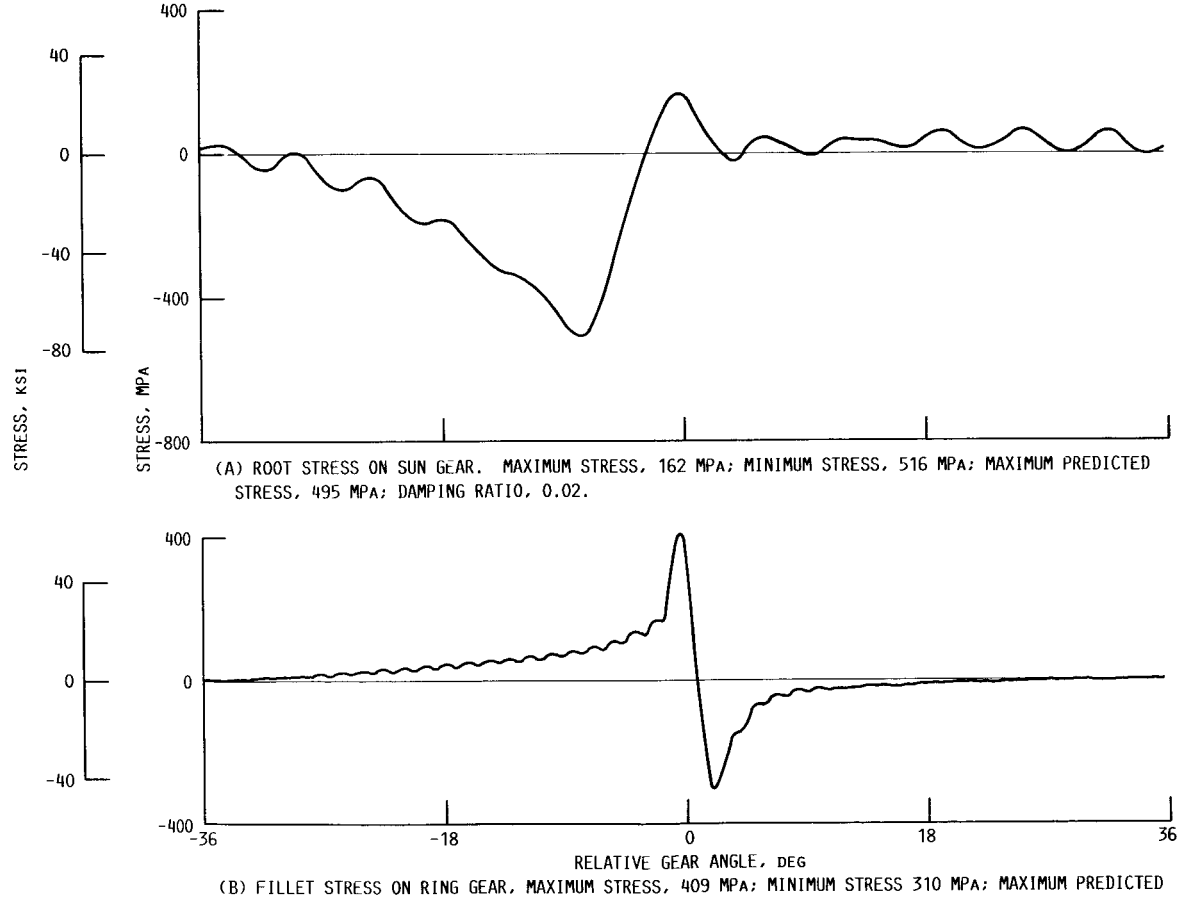

(A) ROOT STRESS ON SUN GEAR. MAXIMUM STRESS, 162 MPA; MINIMUM STRESS, 516 MPA; MAXIMUM PREDICTED STRESS, 495 MPA; DAMPING RATIO, 0.02.

(B) FILLET STRESS ON RING GEAR, MAXIMUM STRESS, 409 MPA; MINIMUM STRESS 310 MPA; MAXIMUM PREDICTED STRESS, 295 MPA; DAMPING RATIO, 0.10.

FIGURE 14. - EXPERIMENTAL DATA ON BENDING STRESSES WITH AVERAGES OF TEN DATA POINTS. SUN GEAR SPEED, 1206 RPM; INPUT TORQUE ON SUN GEAR, 15 000 N-M (11 100 LB-FT).

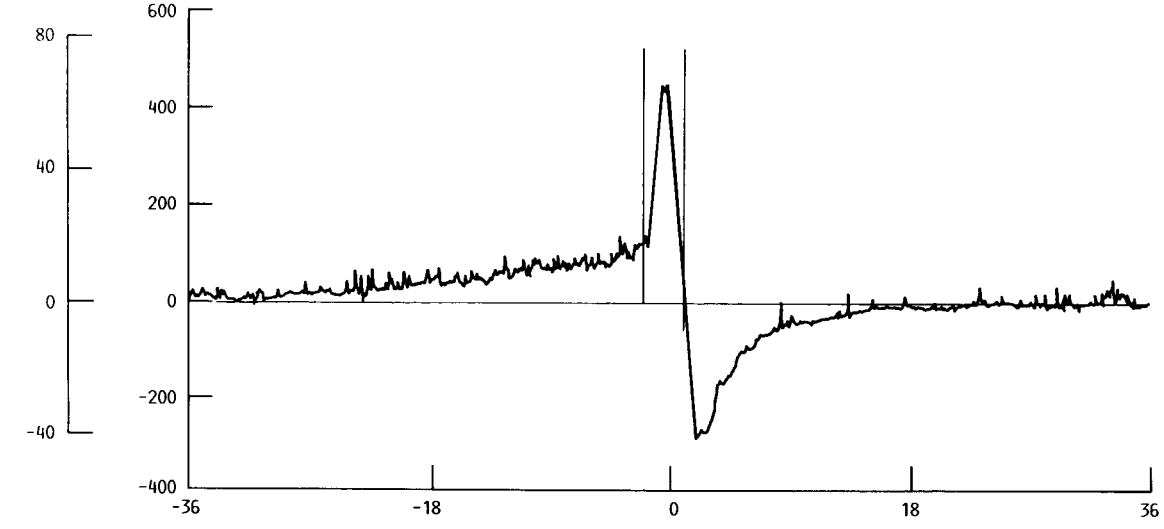

(A) SINGLE TRACE DATA ON RING GEAR BENDING STRESS WITHOUT FILTER.

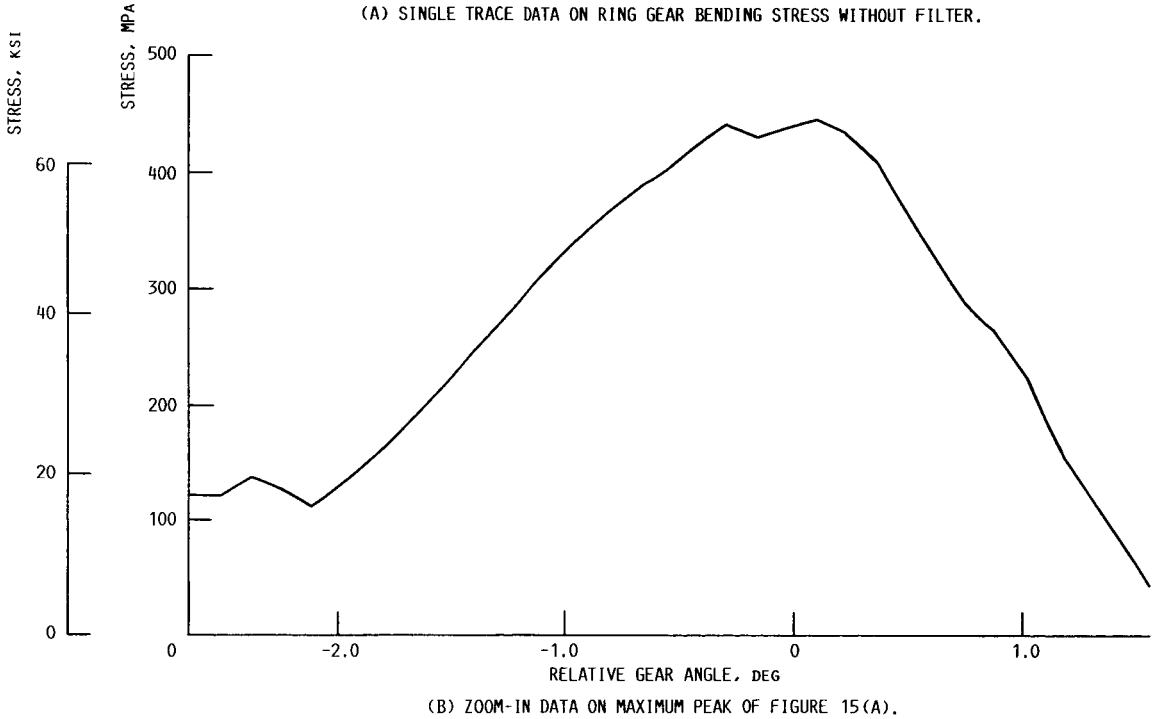

(B) ZOOM-IN DATA ON MAXIMUM PEAK OF FIGURE 15(A).

FIGURE 15. - SINGLE TRACE DATA ON RING GEAR BENDING STRESS WTHOUT FILTER. SUN GEAR SPEED, 1206 RPM; INPUT TORQUE ON SUN GEAR, 15 000 N-M (11 100 LB-FT).

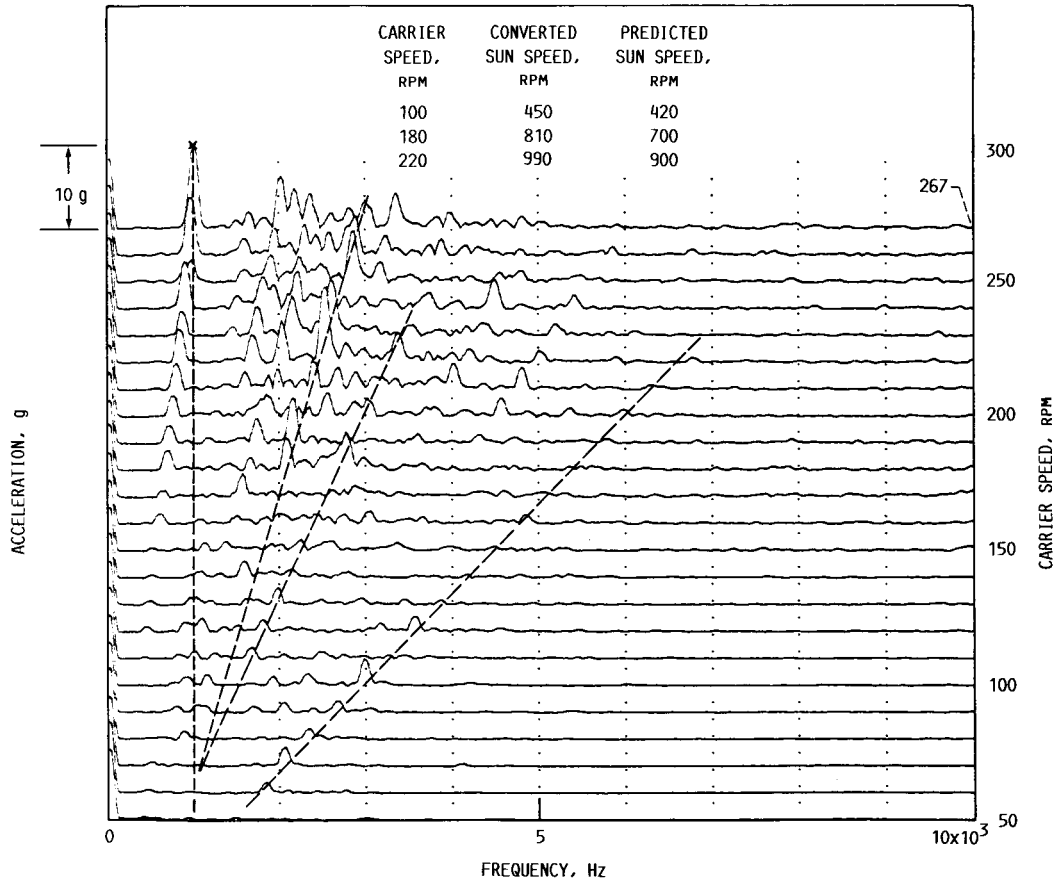

FIGURE 16. - EXPERIMENTAL VIBRATION DATA AT SEVERAL SPEEDS WITH VIBRATION ACCELEROMETER LOCATED NEAR RING GEAR. INPUT TORQUE ON SUN GEAR, 5000 N-M (3700 LB-FT).

1. Report No.	2. Government Accession No.	3. Recipient's Catalog No.
NASA TM-88975		

4. Title and Subtitle	5. Report Date
Experimental and Analytical Evaluation of Dynamic Load and Vibration of a 2240-kW (3000-hp) Rotorcraft Transmission	6. Performing Organization Code: 505-62-51

7. Author(s)	8. Performing Organization Report No.
Fred K. Choy, Dennis P. Townsend, and Fred B. Oswald	E-3380
	10. Work Unit No.

9. Performing Organization Name and Address	11. Contract or Grant No.
National Aeronautics and Space Administration Lewis Research Center Cleveland, Ohio 44135	13. Type of Report and Period Covered: Technical Memorandum

12. Sponsoring Agency Name and Address	14. Sponsoring Agency Code
National Aeronautics and Space Administration Washington, D.C. 20546	

15. Supplementary Notes

Prepared for the Design Engineering Conference and Show, sponsored by the American Society of Mechanical Engineers, Chicago, Illinois, March 2-5, 1987. Fred K. Choy, Summer Faculty Fellow, presently at The University of Akron, Akron, Ohio.

16. Abstract

A dynamic analysis of a 2240-kW (3000-hp) helicopter planetary system is presented. Results from both analytical and experimental studies show good correlation in gear-tooth loads. A parametric study indicates that the mesh damping ratio has a significant effect on maximum gear-tooth load, stress, and vibration. Correlation with experimental results indicates that the sun-planet mesh damping ratio can significantly differ from the planet-ring mesh damping ratio. A numerical fast Fourier transform (FFT) procedure was applied to examine the mesh load components in the frequency domain and the magnitudes of multiple tooth-pass frequencies excited by nonsynchronous meshing of the planets. Effects of tooth-spacing errors and tooth-profile modifications with tip relief are examined. A general discussion of results and correlation with the experimental study are also presented.

17. Key Words (Suggested by Author(s))	18. Distribution Statement
Gearing; Dynamic analysis; Multimesh; Gear dynamics; Gear vibrations; Transmission	Unclassified - unlimited STAR Category 37

19. Security Classif. (of this report)	20. Security Classif. (of this page)	21. No. of pages	22. Price*
Unclassified	Unclassified	17	A02

*For sale by the National Technical Information Service, Springfield, Virginia 22161